



# Examining the universality of the hemolysis power law model from simulations of the FDA nozzle using calibrated model coefficients

Alberto Mantegazza<sup>1</sup> · Nicolas Tobin<sup>1</sup> · Keefe B. Manning<sup>1</sup> · Brent A. Craven<sup>2</sup> 

Received: 24 January 2022 / Accepted: 27 October 2022 / Published online: 23 November 2022  
This is a U.S. Government work and not under copyright protection in the US; foreign copyright protection may apply 2022

## Abstract

Computational fluid dynamics (CFD) is widely used to predict mechanical hemolysis in medical devices. The most popular hemolysis model is the stress-based power law model that is based on an empirical correlation between hemoglobin release from red blood cells (RBCs) and the magnitude of flow-induced stress and exposure time. Empirical coefficients are traditionally calibrated using data from experiments in simplified Couette-type blood-shearing devices with uniform-shear laminar flow and well-defined exposure times. Use of such idealized coefficients in simulations of real medical devices with complex hemodynamics is thought to be a primary reason for the historical inaccuracy of absolute hemolysis predictions using the power law model. Craven et al. (Biomech Model Mechanobiol 18:1005–1030, 2019) recently developed a CFD-based Kriging surrogate modeling approach for calibrating empirical coefficients in real devices that could potentially be used to more accurately predict absolute hemolysis. In this study, we use the FDA benchmark nozzle to investigate whether utilizing such calibrated coefficients improves the predictive accuracy of the standard Eulerian power law model. We first demonstrate the credibility of our CFD flow simulations by comparing with particle image velocimetry measurements. We then perform hemolysis simulations and compare the results with in vitro experiments. Importantly, the simulations use coefficients calibrated for the flow of a suspension of bovine RBCs through a small capillary tube, which is relatively comparable to the flow of bovine blood through the FDA nozzle. The results show that the CFD predictions of relative hemolysis in the FDA nozzle are reasonably accurate. The absolute predictions are, however, highly inaccurate with modified index of hemolysis values from CFD in error by roughly three orders of magnitude compared with the experiments, despite using calibrated model coefficients from a relatively similar geometry. We rigorously examine the reasons for the inaccuracy that include differences in the flow conditions in the hemolytic regions of each device and the lack of universality of the hemolysis power law model that is entirely empirical. Thus, while the capability to predict relative hemolysis is valuable for product development, further improvements are needed before the power law model can be relied upon to accurately predict the absolute hemolytic potential of a medical device.

**Keywords** Hemolysis · Blood damage · Power law model

## 1 Introduction

Mechanical hemolysis is a concern with many blood-contacting medical devices, particularly those that cause large flow-induced stress such as mechanical circulatory support

devices and artificial heart valves. Historically, in vitro experimental testing is performed to evaluate the hemolytic potential of a medical device. In recent years, however, computational fluid dynamics (CFD) has become widely used for predicting mechanical hemolysis (e.g., see Fraser et al. 2012; Goubergrits et al. 2016; Yu et al. 2017; Heck et al. 2017; Tobin and Manning 2020).

Historically, continuum stress-based power law models are the most popular type for macroscale CFD modeling of hemolysis in medical devices. There are a number of different stress-based models that have been formulated, both in Eulerian and Lagrangian frames of reference (e.g., Grigioni et al. 2005; Taskin et al. 2012; Yu et al. 2017). Nearly all of

✉ Brent A. Craven  
brent.craven@fda.hhs.gov

<sup>1</sup> Department of Biomedical Engineering, Pennsylvania State University, University Park, PA, USA

<sup>2</sup> Office of Science and Engineering Laboratories, Center for Devices and Radiological Health, United States Food and Drug Administration, Silver Spring, MD, USA

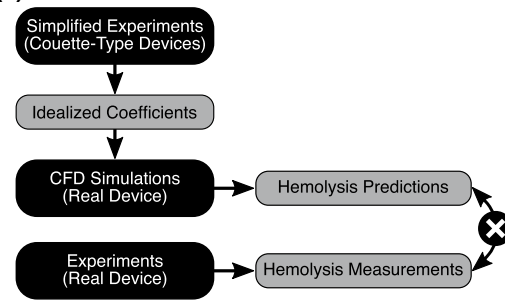
these models are based on an empirical power law correlation proposed by Giersiepen et al. (1990) that relates the amount of hemoglobin released from red blood cells (RBCs) to the exposure time ( $t_{exp}$  [s]) and the magnitude of the flow-induced shear stress ( $\sigma_{shear}$  [Pa]):

$$H = \frac{fHb(1 - H_{ct}/100)}{Hb} = C t_{exp}^a \sigma_{shear}^b \quad (1)$$

Here,  $H$  is the relative fraction of plasma-free hemoglobin to the total blood hemoglobin (i.e., sum of the hemoglobin present inside intact RBCs and plasma-free hemoglobin),  $H_{ct}$  [%] is the hematocrit,  $fHb$  [mg/dl plasma] is the plasma-free hemoglobin concentration,  $Hb$  [mg/dl blood] is the total blood hemoglobin concentration, and  $C$ ,  $a$ , and  $b$  are empirical coefficients. These empirical coefficients are usually determined by performing a statistical regression of Eq. 1 using data from in vitro hemolysis experiments in simplified Couette-type shearing devices in which the blood flow is laminar and experiences uniform-shear conditions with well-defined exposure times (Heuser and Opitz 1980; Zhang et al. 2011; Ding et al. 2015). As illustrated in Fig. 1(a), these idealized coefficients are then used in CFD simulations to predict hemolysis in a complex medical device such as an artificial heart valve or mechanical circulatory support device in which the RBCs experience turbulence, non-uniform shear stress, and also flow-induced extensional stress—all with highly variable exposure times. Such complex hemodynamic flow conditions in real devices are a significant departure from the idealized conditions used to calibrate the model coefficients. As a result, accurately predicting absolute plasma-free hemoglobin levels in medical devices using this traditional approach remains a significant challenge (Taskin et al. 2012; Yu et al. 2017; Craven et al. 2019). Indeed, as concluded by Yu et al. (2017), who compared CFD hemolysis predictions for a rotary blood pump using different sets of traditional model coefficients from simplified experiments and found that the results can vary by a factor of 50, determining better model coefficients “is therefore essential to increase prediction accuracy.”

In an attempt to more accurately predict absolute hemolysis levels, Craven et al. (2019) recently developed an improved approach for calibrating hemolysis power law model coefficients in a real medical device. The approach consists of using CFD to calculate hemolysis generation in a medical device with different sets of power law coefficients ( $C$ ,  $a$ , and  $b$ ). Kriging interpolation is then used to interpolate the CFD results and map the continuous hemolysis solution in three-dimensional ( $C$ ,  $a$ ,  $b$ ) parameter space. The resultant CFD-based Kriging surrogate model solution is compared with experimental measurements for the same device to determine the set of calibrated coefficients that yields hemolysis predictions that

### (a) Traditional Idealized Calibration Approach



### (b) Device-Specific Calibration Approach

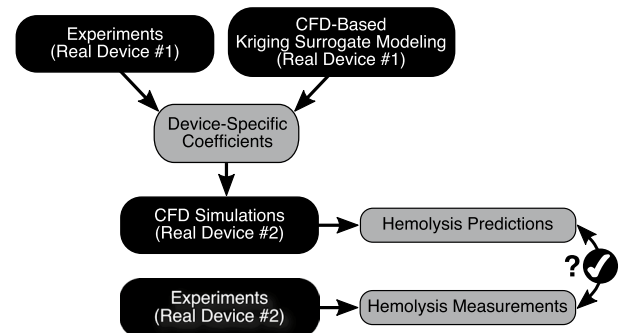


**Fig. 1** a Traditional idealized and b device-specific approaches for calibrating hemolysis power law model coefficients. In the traditional approach (a), model coefficients are obtained by performing a statistical regression of Eq. 1 using data from in vitro hemolysis experiments in simplified Couette-type shearing devices with idealized flow conditions. In the device-specific calibration approach (b) proposed by Craven et al. (2019), CFD-based Kriging surrogate modeling is combined with experimental measurements in a real device to determine the set of calibrated coefficients that yields hemolysis predictions that match the experiments. These calibrated coefficients can then, in theory, be used to more accurately predict hemolysis at different operating conditions of the same medical device or in a completely different device

match the experiments. As illustrated in Fig. 1(b), the calibrated coefficients can then be used to predict hemolysis at different operating conditions of the same medical device or in a completely different device. Compared with using traditional empirical coefficients from simplified experiments (Fig. 1a), this approach should, in theory, improve hemolysis power law model predictions in complex medical devices. The ultimate success of using calibrated coefficients to improve the predictive accuracy, however, depends on the universality of the power law model and the extent of the differences in the hemodynamic flow conditions between the device used for calibration and the device of interest (devices #1 and #2 in Fig. 1(b), respectively). While Craven et al. (2019) developed and verified the approach and demonstrated its use by calibrating coefficients for a capillary tube model, the accuracy of applying calibrated coefficients from one device to another device has yet to be investigated.

The objective of this study is to assess the approach of using calibrated empirical coefficients to improve the predictive accuracy of the hemolysis power law model in a real device. We use the standard Eulerian power law model and calibrated coefficients from Craven et al. (2019) to predict hemolysis in the FDA benchmark nozzle (Malinauskas et al. 2017). We begin by demonstrating the credibility of our CFD simulations of the flow field in the FDA nozzle by comparing with the particle image velocimetry (PIV) measurements of Hariharan et al. (2011). We then perform hemolysis simulations using calibrated coefficients and compare the results with the FDA nozzle hemolysis measurements of Herbertson et al. (2015). Importantly, the calibrated power law coefficients are for the flow of a suspension of bovine RBCs through a 1-mm diameter capillary tube, which is relatively comparable to the flow of bovine blood through the 4-mm diameter FDA nozzle model. Thus, this case represents an ideal test of using calibrated coefficients from one device to predict hemolysis in another similar device using the power law model. If the hemolysis predictions are reasonably accurate, there is hope of using this approach to more accurately predict hemolysis in even more complicated devices. If the predictions are highly inaccurate, however, there is reason to believe that the underlying power law model lacks universality in that it cannot be used to reliably predict the hemolytic potential of a device for which the model has not been calibrated.

## 2 Materials and methods

### 2.1 Geometry

Flow and hemolysis simulations were performed for the FDA nozzle. The flow field characteristics of this benchmark geometry have been investigated experimentally and numerically in a series of interlaboratory studies coordinated by the FDA (Hariharan et al. 2011; Stewart et al. 2012, 2013). A companion in vitro study was also carried out to evaluate the hemolysis generated by the nozzle, which shares design characteristics of blood-contacting medical devices such as syringes, hypodermic needles, and hemodialysis tubing (Herbertson et al. 2015).

In this study, we consider the nozzle oriented with the sudden contraction at the inlet. In this orientation, blood flows from a 12 mm diameter tube, through a sudden contraction into a 4 mm diameter throat, before exiting the model through a conical diffuser (Fig. 2). This produces regions of flow acceleration, deceleration, and recirculation with large variations in the velocity and flow-induced stress that can cause blood damage (Stewart et al. 2013). Ten cross sections were defined along the main flow direction (Fig. 2) where we compare CFD results to the

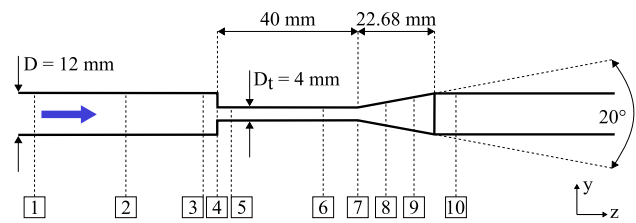


**Fig. 2** FDA benchmark nozzle model in the sudden contraction orientation. Flow is from left to right and enters the throat section through a sharp sudden contraction and exits the throat through a conical diffuser. Ten cross sections are illustrated at  $z = -48, -24, -4, 0, 4, 32, 40, 48, 56, 72$  mm where numerical and experimental results are compared

experimental measurements from the FDA interlaboratory studies (Hariharan et al. 2011; Herbertson et al. 2015).

### 2.2 Validation experiments

To validate the CFD flow simulations, we compare with the interlaboratory experimental PIV data of Hariharan et al. (2011). Briefly, the FDA nozzle (Fig. 2) was connected to a flow loop and a blood analog fluid comprised of 30% water, 20% glycerin, and 50% sodium iodide (by mass) was recirculated by a centrifugal pump. The loop was designed to obtain fully developed inflow to the nozzle. Constant temperature experiments were performed over a range of nozzle throat Reynolds numbers ( $Re_t$ ) from 500 to 6500, spanning laminar to turbulent regimes. Measurements of mean velocity were acquired using 2D planar PIV at the cross sections shown in Fig. 2. Static pressure was also measured using a separate nozzle that included pressure taps.

For hemolysis, we compare CFD predictions with the interlaboratory study of Herbertson et al. (2015), who characterized the hemolytic potential of the FDA nozzle in both sudden and gradual contraction orientations. In the experiments, bovine blood was recirculated through the flow loop and FDA nozzle for two hours with the hematocrit, temperature, blood volume, flow rate, and pressure held constant. Blood samples were collected at incremental time points and centrifuged for plasma isolation. Hemolysis was quantified by measuring the variation of plasma-free hemoglobin concentration ( $fHb$ ) over time via spectrophotometry. In this study, we consider the results obtained for the nozzle orientation that generated the highest hemolysis (sudden contraction orientation as in Fig. 2) and the flow condition for which experimental PIV data are available for validation (flow rate of 5 L/min corresponding to a throat Reynolds number of  $Re_t = 6650 \pm 570$ ). Under these conditions, Herbertson et al. (2015) report a modified index of hemolysis (MIH) value of  $0.292 \pm 0.249$ .

### 2.3 Computational mesh

To perform a CFD mesh refinement study, two pairs of multi-block structured meshes were created using Pointwise (version 18.2). For steady Reynolds-averaged Navier–Stokes (RANS) simulations, two axisymmetric meshes (coarse and fine) were generated that contain approximately 41 thousand and 69 thousand computational cells, respectively. The fine mesh was created by uniformly refining the coarse mesh by a refinement ratio (Roache 2009; Craven et al. 2018) of 1.3. To resolve the large gradients at the wall, a wall-normal spacing of  $1\ \mu\text{m}$  was used in the throat. A high mesh resolution was also used in the entrance to the sudden contraction, in the vicinity of the sharp corner, to resolve large flow-induced stresses in this region where hemolysis is expected to occur.

For large-eddy simulation (LES), two three-dimensional (3D) meshes (coarse and fine) were generated with approximately the same spatial resolution as the corresponding axisymmetric meshes to enable a direct comparison with the RANS simulation results. The coarse and fine 3D meshes contain about 2.4 million and 5.3 million computational cells, respectively. The fine LES mesh (illustrated in Fig. 3) has a refinement ratio of approximately 1.3 relative to the coarse mesh.

To ensure that the LES meshes were adequately refined to resolve the energy-containing turbulence in the FDA nozzle, we estimated the integral turbulence length scale from the results of an initial RANS simulation with the fine axisymmetric mesh using the  $k-\omega$  shear-stress transport (SST) turbulence model (Menter 1994; Menter et al. 2003) (see Secs. 2.4–2.6 for details). Specifically, we calculated an estimate of the integral length scale from the relationship  $l = \sqrt{k}/\beta^*\omega$ , where  $k$  is the turbulent kinetic energy,  $\omega$  is the specific dissipation rate, and  $\beta^* = 0.09$  is a model constant for the  $k-\omega$  SST turbulence model (Menter et al. 2003). The integral scale of turbulence was estimated to be in the range of about  $400\text{--}900\ \mu\text{m}$  in the throat section and  $600\ \mu\text{m}$  or larger in the diffuser, depending on the location. For comparison, the cell sizes for the fine mesh (calculated as the cube root of the cell volume) are in the range of  $20\text{--}105\ \mu\text{m}$  in the throat section and about  $30\text{--}120\ \mu\text{m}$  in the diffuser. The cell sizes for the coarse mesh are approximately  $25\text{--}140\ \mu\text{m}$  in the throat section and about  $40\text{--}155\ \mu\text{m}$  in the diffuser. For reference, we also calculated an estimate of the Kolmogorov length scale as  $\eta = (\nu^3/\epsilon)^{1/4}$  (George 2013), where  $\nu$  is the kinematic viscosity, and  $\epsilon$  is the turbulent kinetic energy dissipation rate that was obtained from the initial RANS simulation. This estimate revealed that the smallest scales of turbulence are in the range of approximately  $20\ \mu\text{m}$ . Therefore, both LES meshes have spatial resolutions of less than about eight times the Kolmogorov length scale and are fine enough to resolve the energy-containing turbulence in the FDA nozzle. Importantly, however, while these estimates provide an initial indication of the adequacy of the

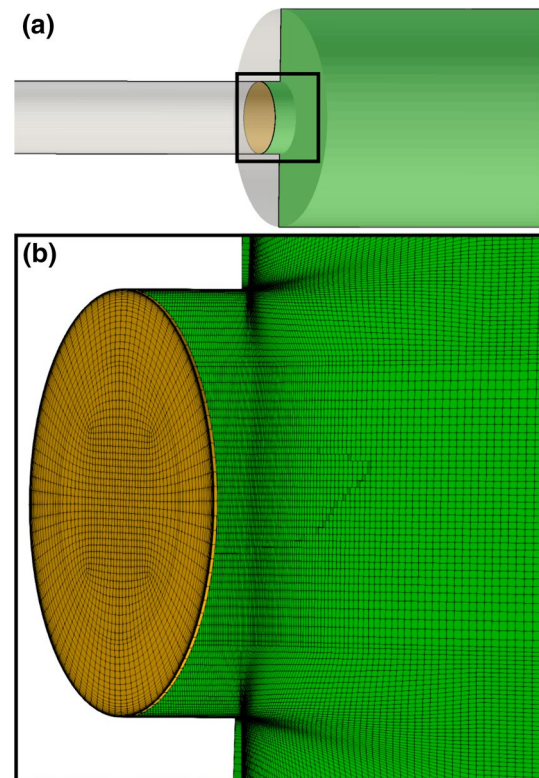


**Fig. 3** Three-dimensional multi-block structured mesh used for large-eddy simulation (LES). **a** Sudden contraction of the FDA nozzle with transverse (orange) and axial (green) planes where mesh cross sections are shown for the **b** fine mesh

LES mesh resolution, we also performed a mesh refinement study using both meshes to ensure that the results of interest are well-resolved.

### 2.4 Governing equations

In this study, we perform both LES and RANS simulations of flow and hemolysis in the FDA nozzle. The LES flow simulations used the wall-adapting local eddy-viscosity (WALE) model (Nicoud and Ducros 1999), while the RANS simulations used the  $k-\omega$  SST turbulence model (Menter 1994; Menter et al. 2003). Blood is an incompressible, non-Newtonian, and shear-thinning fluid, but it behaves as Newtonian when the shear rate is above approximately  $100\ \text{s}^{-1}$  (Merrill and Pelletier 1967; Aycock et al. 2016). For this reason, we modeled blood as a Newtonian fluid in this study.

Following Craven et al. (2019), we use the standard Eulerian power law model for hemolysis simulations:

$$\frac{\partial H'}{\partial t} + (\mathbf{u} \cdot \nabla)H' = (C\sigma^b)^{1/a} \quad (2)$$

where  $H'$  is the linearized plasma-free hemoglobin fraction defined as  $H' = H^{1/a}$ , and  $\sigma$  is the effective scalar stress defined as the magnitude of the resolved viscous stress:

$$\sigma = \sqrt{\frac{1}{2} \boldsymbol{\sigma} : \boldsymbol{\sigma}} \quad (3)$$

where

$$\boldsymbol{\sigma} = \mu(\nabla \mathbf{u} + (\nabla \mathbf{u})^T) \quad (4)$$

is the resolved viscous stress tensor, and  $\mu$  is the dynamic viscosity.

We chose to define  $\sigma$  in this way for several reasons. First, we expect a large majority of the hemolysis in the FDA nozzle to be generated in the region of the sudden contraction where the flow is laminar and RBCs experience extremely large flow-induced viscous stresses. This is supported by the experiments of Herbertson et al. (2015), who measured hemolysis with the FDA nozzle in both orientations (sudden and gradual contraction) under the same flow rate condition (6 L/min) and found that hemolysis generation was nearly two orders of magnitude larger in the sudden contraction orientation. Given that the flow through the nozzle throat and the turbulent jet in the diffuser are relatively similar in both orientations, the large difference in hemolysis is likely due to the extremely large viscous stresses that occur in the sudden contraction where the flow rapidly accelerates. Additionally, we define  $\sigma$  in this way because, as will be described in Sect. 2.7, the model coefficients  $C$ ,  $a$ , and  $b$  are calibrated from experiments and simulations for a similar capillary tube geometry in which the flow is laminar and the same definition of  $\sigma$  is used. Finally, even if there is some minor turbulence-generated hemolysis in the downstream jet of the FDA nozzle, the mechanisms through which turbulence causes damage to RBCs are not well understood and there is not a generally accepted effective scalar stress definition that incorporates the influence of turbulence. For RANS simulations in which turbulent stresses are modeled, it is clear from the literature that it is problematic to simply use the Reynolds stress in defining an effective scalar stress for hemolysis modeling (Hund et al. 2010; Goubergrits et al. 2016; Tobin and Manning 2020). The influence of unresolved turbulence is less of a concern for our LES simulations because our CFD meshes are of high resolution such that the large-scale turbulence and the corresponding viscous stresses are directly resolved.

Given numerical solutions of Eq. 2, a single-pass index of hemolysis can be calculated as the volume-weighted average value of  $H$  through any cross section in the flow domain at which the upstream hemolysis generation has reached steady-state conditions via

$$\text{IH}_{\text{CFD}} = \overline{H}_{\text{CFD}} = \frac{\int_A (H\mathbf{u}) \cdot d\mathbf{A}}{\int_A \mathbf{u} \cdot d\mathbf{A}} \quad (5)$$

where  $d\mathbf{A}$  is the area normal vector of the cross section  $A$ . For all hemolysis simulations reported in this study, we compute  $\text{IH}_{\text{CFD}}$  at a cross section in the FDA nozzle located at  $z = 48$  mm, which corresponds to cross section 8 in Fig. 2. To directly compare CFD predictions of  $\text{IH}_{\text{CFD}}$  with the measurements of Herbertson et al. (2015) who report values of MIH from multi-pass experiments, we compute an equivalent value of MIH from CFD as:

$$\text{MIH}_{\text{CFD}} = 10^6 \text{IH}_{\text{CFD}}. \quad (6)$$

For more information on the definition and derivation of these hemolysis indices, the reader is referred to Craven et al. (2019).

## 2.5 Fluid properties and boundary conditions

In this study, we compare with the FDA interlaboratory experimental data in which the velocity field and hemolysis were measured in separate experiments at conditions corresponding to a blood flow rate of 5 L/min through the nozzle. To directly compare simulations with both the PIV (Hariharan et al. 2011) and the hemolysis (Herbertson et al. 2015) measurements, the CFD fluid properties and boundary conditions were specified to match conditions for each specific experiment. In all cases, the fluid is treated as Newtonian.

For CFD simulations of the flow that are compared with PIV, the fluid density ( $\rho$ ), viscosity ( $\mu$ ), and the inlet flow rate ( $Q$ ) were specified in accord with Stewart et al. (2012) using  $\rho = 1056$  kg/m<sup>3</sup>,  $\mu = 3.5$  cP, and  $Q = 6.77 \times 10^{-5}$  m<sup>3</sup>/s. This yields a throat Reynolds number ( $Re_t$ ) of 6500, which corresponds to the highest flow rate PIV experimental condition (Hariharan et al. 2011). For the hemolysis simulations, the properties and flow rate were set to correspond to the bovine blood properties and the flow rate reported by Herbertson et al. (2015). Specifically, we used values of  $\rho = 1040$  kg/m<sup>3</sup>,  $\mu = 4.24$  cP, and  $Q = 5$  L/min, which yields a throat Reynolds number ( $Re_t$ ) that is the same as in the PIV experiments.

For all simulations, a parabolic velocity profile was prescribed throughout the entire computational domain as an initial condition. A laminar fully developed inlet velocity boundary condition was used, which is consistent with the PIV measurements at this location (Hariharan et al. 2011). To allow for the possibility of reversed flow at the outlet, the pressureInletOutletVelocity condition available in OpenFOAM was used for velocity, which applies a zero-gradient Neumann condition on patch faces where the flow is exiting the domain and an extrapolated Dirichlet condition on faces where there is local inflow. A zero-gradient

pressure boundary condition was imposed at the inlet of the nozzle, and a zero-pressure condition was prescribed at the outlet. For hemolysis simulations, we imposed  $H = 0$  as the initial condition and as the inlet boundary condition. A zero-gradient Neumann condition was used for  $H$  on the walls and the outlet.

## 2.6 Numerical methods

CFD simulations were performed with OpenFOAM (version 7). For both RANS and LES, solutions were computed using the coarse and fine meshes described in Sec. 2.3 to examine the influence of mesh resolution on the results. The simulations were performed on the Expanse high-performance computing (HPC) system at the San Diego Supercomputer Center. Post-processing and visualization of the results utilized Python and the open-source software ParaView.

Steady axisymmetric RANS simulations of the flow were performed using the  $k-\omega$  SST turbulence model (Menter 1994; Menter et al. 2003) with the “consistent” formulation of the Semi-Implicit Method for Pressure-Linked Equations (SIMPLE) algorithm, or SIMPLEC, using second-order accurate discretization schemes. Iterative convergence of the steady-state flow solution was assessed by ensuring that the normalized residuals were less than  $10^{-10}$  and by monitoring minimum and maximum values of the primitive solution variables and integrated quantities such as the average inlet pressure and the outlet flow rate. Given the computed flow solution, Eq. 2 was numerically solved using a custom solver developed and verified in previous work (Craven et al. 2019). Quasi-steady hemolysis solutions were computed with second-order accurate spatial discretization schemes and the SLTS local time discretization scheme available in OpenFOAM with a maximum local Courant number of 0.1. Quasi-steady solution convergence was evaluated by monitoring  $H'$  field values and values of  $MIH_{\text{CFD}}$  (Eq. 6) at a cross section in the nozzle located at  $z = 48$  mm (cross section 8 in Fig. 2). The RANS simulations were performed on four CPU cores and required approximately 70 minutes to compute flow and hemolysis solutions using the coarse axisymmetric mesh and about 112 minutes for the fine mesh.

Time-resolved LES computations of the flow and hemolysis were performed with the custom OpenFOAM solver of Craven et al. (2019) using the pressure-based PIMPLE (hybrid PISO/SIMPLE) algorithm. We used the WALE model (Nicoud and Ducros 1999) for sub-grid scale (SGS) closure, as in previous work (Tobin and Manning 2020), due to its capability to accurately model laminar, transitional, and turbulent flow, all of which exist in the FDA nozzle at the conditions corresponding to a throat Reynolds number of 6500. Second-order accurate discretization schemes were used, including second-order backward for time discretization and central differencing for the advection

of momentum. Adaptive time stepping was used in which the time step size is automatically adjusted to maintain a maximum Courant number of 0.9. LES computations of the flow alone were first run for  $t = 50$  ms to achieve a statistically stationary quasi-steady turbulent flow before starting the combined flow-hemolysis simulation, which was then run until  $t = 100$  ms. The solution variables and values of  $MIH_{\text{CFD}}$  were time-averaged throughout the quasi-steady period. The coarse mesh LES computation was performed on 64 CPU cores and required about 18 days and the fine mesh simulation used 128 CPU cores and required roughly 39 days.

## 2.7 Calibrated empirical hemolysis power law coefficients

We use calibrated power law coefficients from Craven et al. (2019) to predict hemolysis in the FDA nozzle. Specifically, we use the coefficients of  $C = 2.875 \times 10^{-10}$ ,  $a = 0.5$ , and  $b = 2.65$  that were calibrated to match the experimental hemolysis measurements of Kameneva et al. (2004) using CFD-based Kriging surrogate modeling (Craven et al. 2019). Importantly, these coefficients were calibrated for laminar developing flow of a suspension of bovine RBCs through a 1-mm diameter capillary tube, which is relatively comparable to the flow of bovine blood through the 4-mm diameter FDA nozzle. While the throat Reynolds number ( $Re_t$ ) in the FDA nozzle is above the theoretical threshold for turbulence, the developing flow that enters the sudden contraction is laminar before the flow transitions to turbulence downstream. This is important because, as discussed in Sec. 2.4, we expect a large majority of the hemolysis in the FDA nozzle to be generated in the region of the sudden contraction, where the flow is laminar and RBCs experience extremely large flow-induced viscous stresses as the blood rapidly accelerates around the sharp entry corner. Thus, compared with traditional idealized empirical coefficients from simplified Couette-type shearing devices, these calibrated coefficients are ideally suited for predicting hemolysis in the FDA nozzle. For this reason, the present study is an ideal test of using calibrated coefficients from one device to predict hemolysis in another similar device using the power law model.

## 3 Results

### 3.1 Validation of flow in the FDA nozzle

To validate our CFD simulations of flow through the FDA nozzle, we compare with the interlaboratory PIV measurements of Hariharan et al. (2011) for the highest flow rate condition ( $Re_t = 6500$ ) with the nozzle in the sudden

contraction orientation. The comparison includes velocity profiles at various locations in the nozzle, the velocity distribution along the centerline, and the axial distribution of wall pressure from both LES and RANS using the coarse and fine meshes described in Sec. 2.3. In Appendix 1, we provide a detailed description of the CFD mesh refinement and PIV validation studies. For brevity, here we summarize the important results.

Overall, both LES and RANS compare reasonably well with the PIV measurements, except at two locations: (i) in the near-wall region of the sudden contraction where there is large uncertainty in the experimental data that makes a direct comparison difficult and (ii) in the downstream diverging section of the nozzle where RANS significantly underpredicts the spreading rate of the jet and overpredicts the centerline velocity magnitude compared with PIV and LES. As discussed in Appendix 1, the large uncertainty in the near-wall PIV data at the sudden contraction made it challenging to rigorously validate the CFD velocity predictions at this location. As justified, however, because the flow is laminar at the sudden contraction and both LES and RANS predict extremely similar mesh-insensitive solutions here, we believe that this further supports the credibility of the flow simulations in this critical region where a majority of the hemolysis is expected to occur.

Summarizing the mesh refinement study, we found that velocity and wall pressure predictions from the coarse and fine mesh RANS simulations are indistinguishable from one another. For LES, the fine mesh yields slightly more accurate velocity and pressure predictions than the coarse mesh. We also performed a mesh refinement study for hemolysis using the calibrated power law coefficients and found that

predictions of MIH from both RANS and LES are fairly mesh insensitive at this level of refinement, especially in comparison to the corresponding experimental measurements (see Appendix 1 for details). Based on these results, we thus chose the fine meshes to perform all subsequent analyses and simulations.

### 3.2 Predictions of absolute hemolysis in the FDA nozzle

To compare LES and RANS hemolysis simulations, we first consider the distribution of the predicted hemolysis in the nozzle. Contours of the mean relative plasma-free hemoglobin concentration ( $H_{mean}$ ) are shown in Fig. 4(a,b) from simulations with the fine meshes using the calibrated power law coefficients. Here, we see that both LES and RANS predict comparable maximum concentrations just downstream of the sudden contraction along the wall. In the LES case, the plasma-free hemoglobin quickly disperses downstream in the throat due to turbulent mixing. In the RANS simulation, however, the  $H_{mean}$  field remains confined to the wall as it advects downstream without cross-stream transport due to the lack of both molecular and turbulent diffusion terms in the Eulerian power law model. This has important implications for hemolysis modeling because it means that simulations using RANS-based turbulence models with the standard Eulerian power law model do not accurately predict the spatial distribution of plasma-free hemoglobin in the blood flow. Even so, this limitation of the RANS hemolysis simulation does not affect the overall index of hemolysis prediction because the steady-state, flow-weighted  $MIH_{CFD}$  calculation

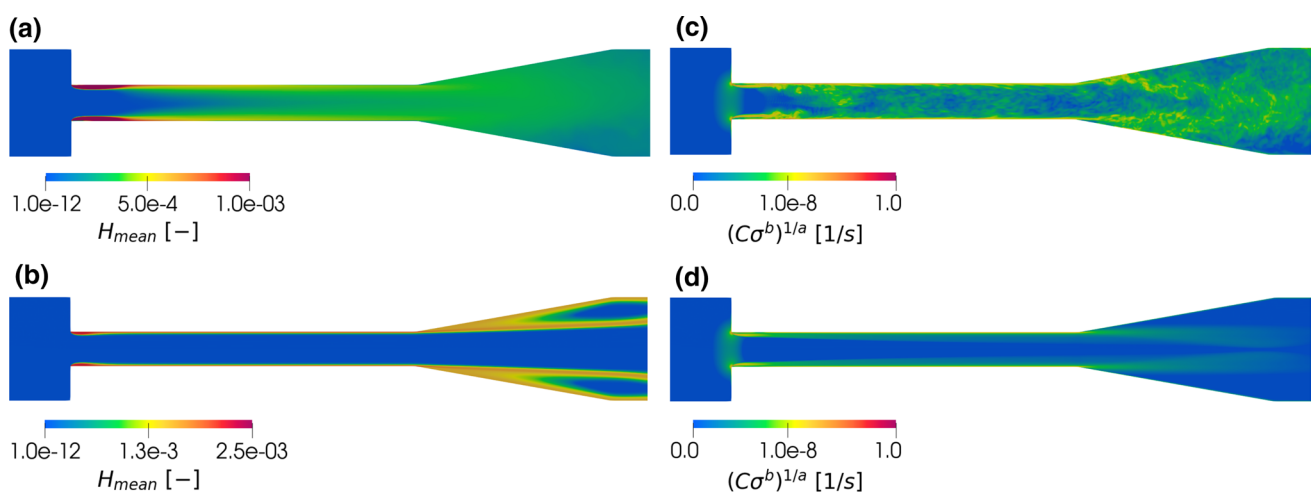


**Fig. 4** CFD predictions of hemolysis in the FDA nozzle at  $Re_t = 6500$  using the standard Eulerian power law model with calibrated empirical coefficients from Craven et al. (2019). Contour plots of the mean relative plasma-free hemoglobin concentration ( $H_{mean}$ ) in

the nozzle from **a** LES and **b** RANS. Contours of the magnitude of the hemolysis power law model source term  $((C\sigma^b)^{1/a})$  from **c** LES and **d** RANS

(Eq. 6) is not sensitive to the spatial distribution of the  $H_{mean}$  field for a given total upstream hemolysis generation.

To investigate where a majority of the predicted hemolysis generation occurs in the FDA nozzle, we consider contours of the power law model source term  $(C\sigma^b)^{1/a}$  in Fig. 4(c,d). Interestingly, we see that LES predicts that some hemolysis is generated by resolved turbulent viscous stresses downstream in the core of the nozzle throat (Fig. 4c), while RANS predicts that hemolysis is only generated in the near-wall region and the shear layer of the turbulent jet in the diffuser section (Fig. 4d). Importantly, however, the magnitude of generation due to turbulence is extremely small compared to that in the sudden contraction. Both LES and RANS predict comparable distributions of generation in the sudden contraction where the flow is laminar, with the highest levels occurring at the inlet corner where the blood flow accelerates around the sharp 90° bend. As illustrated, the levels of generation here are roughly eight orders of magnitude greater than anywhere else in the nozzle, including the turbulent jet. This, therefore, provides strong a posteriori justification of our choice of using empirical model coefficients calibrated for laminar flow through a small capillary tube (see Sec. 2.7).

The CFD predictions of MIH are compared with the experimental measurements of Herbertson et al. (2015) in Fig. 5. Here, we see that, using the calibrated coefficients, LES and RANS yield MIH values of 421 and 210, respectively. As previously noted, the difference in the two CFD solutions is largely due to the fact that LES predicts some hemolysis generation by resolved turbulent viscous stresses in the core of the flow, while RANS does not. Compared with the experiments, however, this difference

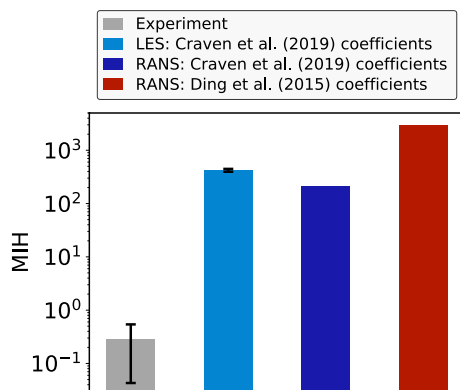


**Fig. 5** CFD predictions of the modified index of hemolysis (MIH) for the FDA nozzle in the sudden contraction orientation with a blood flow rate of 5 L/min compared with the experimental measurements of Herbertson et al. (2015) with bovine blood (shown as mean  $\pm$  SD). The CFD simulations use power law model coefficients from Craven et al. (2019) that were calibrated for the flow of a suspension of bovine RBCs through a small capillary tube (see Sec. 2.7). Error bars for LES represent the time-averaged mean  $\pm$  SD

is insignificant, as both CFD predictions differ from the experimental MIH of  $0.292 \pm 0.249$  by roughly three orders of magnitude.

Finally, we investigate whether using calibrated empirical coefficients from the capillary tube improves the predictive accuracy of the power law model compared with the traditional approach of using coefficients derived from in vitro hemolysis experiments in simplified Couette-type shearing devices with idealized flow conditions. As a test, we performed an additional hemolysis simulation of the FDA nozzle with our axisymmetric RANS model using the only set of traditional coefficients available in the literature for bovine blood, which are those of Ding et al. (2015):  $C = 9.772 \times 10^{-7}$ ,  $a = 0.2076$ , and  $b = 1.4445$ . As shown in Fig. 5, the CFD simulation using the traditional coefficients predicted an MIH value of 2974, more than an order of magnitude larger than the MIH of 210 from the calibrated coefficient RANS simulation and in error compared to the experimental MIH of 0.292 by more than four orders of magnitude. Thus, compared with the traditional approach, the present calibration approach is an improvement, though the absolute hemolysis predictions are still highly inaccurate despite using model coefficients that were calibrated for the flow of a suspension of bovine RBCs through a relatively similar capillary tube geometry.

### 3.3 Predictions of relative hemolysis in the FDA nozzle

As a final test of the Eulerian power law model, we consider the accuracy of *relative* hemolysis predictions for the FDA nozzle by comparing with additional experimental data with the nozzle in both the sudden contraction and gradual contraction orientations at different flow rates. Herbertson et al. (2015) conducted three separate sets of experiments with the FDA nozzle using bovine blood: sudden contraction (SC) orientation at 5 L/min (the case that we have considered thus far), gradual contraction (GC) orientation at 6 L/min, and SC orientation at 6 L/min. Using our axisymmetric RANS CFD model with the fine mesh, we replicate each of these three tests by switching the model orientation and changing the flow rate. As before, for each case, we performed a steady simulation of the flow using the  $k-\omega$  SST turbulence model followed by a quasi-steady hemolysis simulation using the calibrated power law coefficients. Given the results, we compare relative hemolysis predictions with the experiments, both in terms of the rank ordering of the three conditions and by comparing quantitative values of relative MIH that are calculated by normalizing the absolute MIH value for each case by the respective value for condition 2 (GC at 6 L/min).

As illustrated in Fig. 6, we see that CFD does accurately reproduce the rank ordering of the relative hemolysis levels across the three conditions. That is, CFD predicts hemolysis

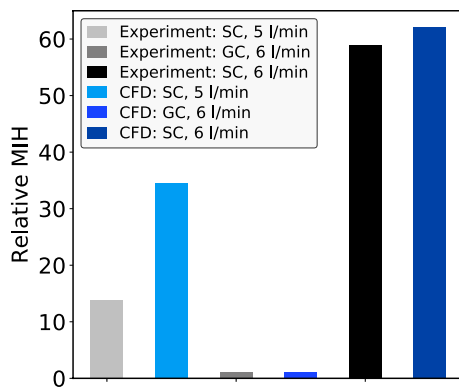


**Fig. 6** CFD predictions of relative MIH compared with the experimental measurements of Herbertson et al. (2015) for the FDA nozzle with bovine blood in the sudden contraction (SC) and gradual contraction (GC) orientations at flow rates of either 5 L/min or 6 L/min. The CFD results are from axisymmetric RANS simulations using calibrated power law coefficients from Craven et al. (2019). Relative MIH is calculated by normalizing the absolute value for each case by the respective MIH from either the experiments or CFD for the second condition (GC at 6 L/min)

to be least at condition 2 (GC at 6 L/min) and greatest at condition 3 (SC at 6 L/min), with condition 1 falling in between, which generally corresponds with the experiments. Quantitatively, the relative MIH from CFD for condition 1 (SC at 5 L/min) is 34.6 compared to a value of 13.9 from the experiments. At condition 3 (SC at 6 L/min), CFD predicts a relative MIH of 62 that is in close agreement with the value of 59 from the experiments. Thus, given the inaccuracy of the absolute predictions, the relative hemolysis CFD predictions are quite good.

### 3.4 Comparison of FDA nozzle and capillary tube used for calibration

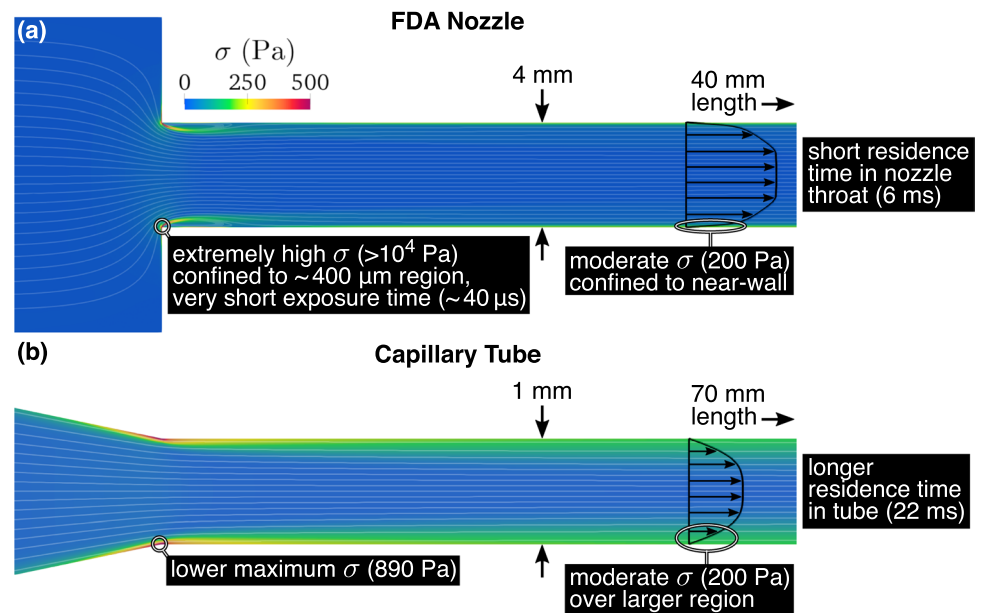
To understand the reasons for the inaccuracy of the absolute hemolysis CFD predictions, we compare the flow and stress fields in the FDA nozzle with that in the 1-mm diameter capillary tube that was used to calibrate the empirical power law coefficients. Here, we consider CFD results of the capillary tube of Kameneva et al. (2004) from previously reported simulations (Craven et al. 2019). We specifically consider the lowest flow rate capillary tube case of Kameneva et al. (2004) because it yields an average wall shear stress that is most comparable with that experienced in the FDA nozzle in the sudden contraction orientation at a blood flow rate of 5 L/min. In comparing the FDA nozzle and the capillary tube, we examine several hemolysis-related quantities from the CFD simulations that include the velocity magnitude, effective flow-induced scalar stress (Eq. 3), magnitude of the power law model source term ( $(C\sigma^b)^{1/a}$ ), extensional stress, and the residence time. In Appendix 2, we provide a detailed

comparative analysis of these quantities in each device. For brevity, here we summarize the important results that help to answer two important questions.

First, why did separate experiments performed with each device show that the capillary tube is more hemolytic than the FDA nozzle? At first thought, one might expect the FDA nozzle to be more hemolytic due to the higher Reynolds number and the fact that the flow is turbulent in much of the model. At these conditions, however, that is not the case, as the average measured MIH value for the capillary tube is estimated to be 8.31 (Craven et al. 2019) compared to 0.292 for the FDA nozzle (Herbertson et al. 2015). As illustrated in Fig. 7, this is likely due to several significant differences in the fluid dynamics for each device. In the FDA nozzle, extremely high flow-induced stresses in excess of  $10^4$  Pa occur in the inlet, but they are confined to a very small region at the sharp inlet corner. Because of the high velocity at the inlet corner, the local exposure time to these high stresses is very brief. From the CFD simulations, the high stresses occur over a length scale of approximately  $400 \mu\text{m}$  and where the flow speed is in the range of 10 m/s, yielding a local exposure time of approximately  $40 \mu\text{s}$ . Downstream in the throat section of the nozzle, the stresses are much lower (in the range of 200 Pa) and are confined to a thin region next to the wall, where there is little flow due to the no-slip condition. Stresses in the shear layer of the downstream jet are even lower: approximately 150 Pa as the jet forms at the entrance to the diffuser and dropping precipitously to 50 Pa over a downstream distance of about 3 mm as the jet expands. As previously postulated, for this reason, most of the hemolysis generation likely occurs in the nozzle inlet where exposure times are very brief, which limits the amount of hemolysis generation in the device. This is further supported by the experiments of Herbertson et al. (2015), who measured hemolysis with the FDA nozzle in both orientations (sudden and gradual contraction) under the same flow rate condition (6 L/min). They found that hemolysis generation was nearly two orders of magnitude larger in the sudden contraction orientation, “suggesting that the sharp corner geometry of the sudden-contraction inlet was the primary source of blood damage” (Herbertson et al. 2015). Given that the flow through the nozzle throat and the turbulent jet in the diffuser are relatively similar in both orientations, as noted by Herbertson et al. (2015), this is likely due to the extremely large viscous stresses that occur in the sudden contraction where the flow rapidly accelerates around the sharp inlet corner.

In contrast, the capillary tube has much lower flow-induced stresses at the inlet, but a much larger region of moderate shear stress along the wall. The moderate stresses along the wall are in the range of 200 Pa and occur over a much larger radial extent compared to the nozzle (see Fig. 7). Because the capillary tube is also significantly

**Fig. 7** Flow-induced viscous scalar stress field ( $\sigma$ ) in the **a** FDA nozzle from RANS CFD simulations compared with that in the **b** 1-mm diameter capillary tube that was used to calibrate the empirical hemolysis power law coefficients used in this study. The FDA nozzle is in the sudden contraction orientation with a blood flow rate of 5 L/min, which yields approximately the same average wall shear stress (200 Pa) as in the lowest flow rate capillary tube case of Kameneva et al. (2004) (see the main text for details)



longer, this yields a much larger volume of blood that is exposed to moderate flow-induced stress for a comparatively long residence time relative to the nozzle. As detailed in Appendix 2, the average residence time for blood to flow through the 70-mm-long capillary tube is approximately 22 ms compared to about 6 ms for blood to flow through the 40-mm-long throat section of the FDA nozzle. Longer exposure time to moderate shear stress over a larger region likely explains why the capillary tube is more hemolytic. Additionally, as detailed in Appendix 2, the capillary tube has a larger region of low-to-moderate extensional stress in the inlet (e.g., in the range of 10–50 Pa). Faghih and Sharp (2020) found that RBCs deform much more under extensional stress than shear stress. While the hemolytic potential of extensional stress has yet to be thoroughly investigated, if such low-to-moderate levels cause damage to RBCs, this could also help to explain the higher measured hemolysis levels in the capillary tube.

The second related question we consider here is: why are the absolute hemolysis CFD predictions in the FDA nozzle in this study so inaccurate using model coefficients calibrated from the capillary tube? We believe this is fundamentally because the flow-induced stress distribution and exposure times in the hemolytic regions of each device are quite different, as demonstrated here. The model coefficients were calibrated by Craven et al. (2019) from CFD simulations of the capillary tube for three flow conditions with wall shear stresses of 200–400 Pa and average residence times in the tube in the range of 10–20 ms. The moderate stresses in the capillary occur over a relatively large spatial extent. The model coefficients are then applied in this study to predict hemolysis in the FDA nozzle in the sudden

contraction orientation, in which much of the blood damage is predicted to occur in a very small region at the sharp inlet corner where the stresses are extremely high ( $\sim 10^4$  Pa) and local exposure times are very brief (about 40  $\mu$ s). Thus, while the geometries are relatively similar and the average wall shear stresses are comparable, the flow-induced stress and exposure time *in the hemolytic regions* vary substantially between the two devices. Given the simple empirical nature of the hemolysis power law model, these significant differences between the calibration and application conditions lead to a significant overprediction of hemolysis in the FDA nozzle.

## 4 Discussion

Our results show that the Eulerian power law model yields reasonably accurate CFD predictions of relative hemolysis in the FDA nozzle, but highly inaccurate predictions of absolute hemolysis despite using model coefficients that were calibrated using a relatively similar device. This is generally in accord with Taskin et al. (2012), who used traditional empirical coefficients from the literature with the same power law model and similarly obtained inaccurate CFD predictions of absolute hemolysis, but more reliable relative hemolysis predictions for a clinical ventricular assist device (VAD) and a custom axial blood-shearing device based on a commercial blood pump. In this study, however, we used empirical coefficients that were calibrated for the flow of a suspension of bovine RBCs through a 1-mm diameter capillary tube, which is relatively comparable to the flow of bovine blood through the 4-mm diameter FDA nozzle. The

objective is to assess whether using such calibrated coefficients significantly improves the predictive accuracy of absolute hemolysis levels. As shown here, it does not, as our predictions of MIH differ from the experiments by roughly three orders of magnitude.

A main reason why the Eulerian power law model fails to accurately predict absolute hemolysis is that the flow conditions differ in the hemolytic regions of the devices used for calibration and application. In this study, we used model coefficients that were calibrated for a small capillary tube in which moderate stresses of approximately 200–400 Pa occur over a relatively large spatial extent and with exposure times in the range of 10–20 ms. The calibrated coefficients were then applied to predict hemolysis in the FDA nozzle, in which much of the blood damage is predicted to occur in a very small region at the sharp inlet corner where the stresses are extremely high ( $\sim 10^4$  Pa) and local exposure times are very brief (about 40  $\mu$ s). Thus, despite the geometric similarities between the two devices and the fact that the average wall shear stress is comparable, there are significant differences in the distribution of the flow-induced stress and exposure time in the hemolytic regions. These differences lead to a significant overprediction of absolute hemolysis in the FDA nozzle.

Compared with using traditional empirical coefficients derived from simplified Couette-type shearing devices with idealized flow conditions, however, the present device-specific calibration approach is an improvement. As a test, we performed an additional hemolysis CFD simulation of the FDA nozzle using the only set of traditional coefficients available in the literature for bovine blood (Ding et al. 2015), which yielded an absolute MIH value of 2974 that is more than an order of magnitude larger than the MIH of 210 from the calibrated coefficient CFD simulation and in error compared to the experimental MIH of 0.292 by more than four orders of magnitude. Thus, compared with the traditional approach, the present calibration approach is an improvement, though the absolute hemolysis predictions are still highly inaccurate.

The primary underlying reason for the inaccuracy of the hemolysis power law model is that it is entirely empirical and does not include any physics-based mechanisms that cause damage to RBCs. This is likely why the model lacks universality and cannot be applied across a wide range of conditions. As a result, in order to obtain accurate absolute predictions, it is apparent from this study that one must calibrate the power law coefficients under conditions that closely match those in the hemolytic region(s) of a device. Our simulations used calibrated coefficients derived from experiments in a capillary tube with flow-induced stresses of 200–400 Pa and exposure times in the range of 10–20 ms. While these calibration conditions differ from those in the FDA nozzle, they are closer and less idealized than the flow

conditions in the Couette-type shearing devices used to calibrate most traditional coefficients. For example, the blood-shearing experiments of Zhang et al. (2011) span shear stress and exposure time values of 30–320 Pa and 30–1500 ms, respectively, and those of Ding et al. (2015) span similar ranges (25–320 Pa and 40–1500 ms, respectively). Additionally, blood flow in Couette-type shearing devices experiences a constant and uniform shear stress, which is a significant departure from the complex hemodynamics in the FDA nozzle. This is likely why our calibrated coefficient simulations of the FDA nozzle were more accurate than the hemolysis simulation using traditional coefficients. While we could likely obtain even more accurate absolute hemolysis predictions for the FDA nozzle by calibrating coefficients under extremely high stress-short exposure time conditions similar to those in the nozzle inlet, such data are unavailable. Given the simple empirical nature of the power law model, however, even if such data were available, the resultant calibrated coefficients likely could not be successfully applied to other devices with appreciably different conditions (e.g., mechanical heart valve or VAD) or to devices with multiple hemolytic regions with disparate flow conditions.

Nevertheless, we show here that the power law model can be used to make reasonably accurate predictions of relative hemolysis, which is valuable for product development. For instance, relative predictions can be used to optimize a device design or to analyze the impact of small design modifications to a current device. The inability, however, to predict accurate absolute hemolysis levels precludes its use as a primary source of evidence for evaluating device safety.

We believe there are two potential paths forward for more accurately predicting absolute hemolysis levels in medical devices. Given the simplicity and popularity of the power law model, it is potentially feasible to improve its predictive accuracy by establishing a large library of calibrated coefficients that span the wide range of flow conditions that occur in medical devices. Such a library would allow CFD analysts to use an appropriate set of calibrated coefficients based on the predicted flow conditions in their device. Alternatively, a more promising approach is to develop an improved physics-based macroscale hemolysis model that better captures the flow-induced mechanisms that damage RBCs—e.g., by accounting for damage from both extensional and shear stress, predicting whether RBCs instantaneously rupture or accumulate sublytic membrane damage, including damage caused by small-scale turbulence, and incorporating differences in size and mechanical fragility of RBCs for different animal species. Such an improved macroscale model will certainly have empirical coefficients that must be calibrated. Unlike the power law model, however, because the model is physics-based, the empirical coefficients should be more universal such that they can be applied across a wide range of

conditions. We believe that this is the most promising path forward for more accurately predicting absolute hemolysis in medical devices.

Finally, we note some limitations of the study. The hemolysis measurements that we used for calibration in the capillary tube and those for validation in the FDA nozzle are from separate experiments using different bovine blood pools. Further, the capillary tube experiments (Kameneva et al. 2004) used washed bovine RBCs suspended in 10% dextran solution compared with whole bovine blood in the FDA nozzle experiments (Herbertson et al. 2015), which could have some influence on the results reported here. Ideally, model calibration and validation should be performed using experiments conducted with the same blood pool to eliminate this source of variability. Such data, however, are unavailable. In future work, more high-quality experimental hemolysis data are needed in multiple devices using the same blood pool to rigorously calibrate and validate hemolysis models.

Another limitation of the study is that we do not explore the several different possible ways to define the effective scalar stress,  $\sigma$ , in the power law model. Here, we use a common definition of  $\sigma$  that is defined as the magnitude of the resolved viscous stress (Eq. 3). There are, however, several other possibilities that we do not explore, as it was beyond the scope of the present study. As justified in Sec. 2.4, we chose this particular definition of  $\sigma$  for several reasons. First, a large majority of the hemolysis in the FDA nozzle is thought to be generated in the region of the sudden contraction where the flow is laminar and RBCs experience extremely large flow-induced viscous stresses, which is supported by the experiments of Herbertson et al. (2015). Additionally, the empirical power law coefficients that we use in this study were calibrated in previous work (Craven et al. 2019) from experimental data for a capillary tube in which the flow is laminar and the same definition of  $\sigma$  was used. Though there is likely some turbulence-generated hemolysis in the FDA nozzle, the mechanisms through which turbulence causes damage to RBCs are not well understood and there is not a generally accepted effective scalar stress definition that incorporates the influence of turbulence and corresponding empirical coefficients that have been appropriately calibrated with turbulent flow experimental data. For RANS hemolysis simulations in which turbulent stresses are modeled, it is clear from the literature that it is problematic to simply use the Reynolds stress in defining  $\sigma$  (Hund et al. 2010; Goubergrits et al. 2016; Tobin and Manning 2020). This is not surprising because the Reynolds stress is not a physical stress that RBCs experience, but is “simply a re-worked version of the fluctuating contribution to the non-linear acceleration terms” that arises from Reynolds averaging the Navier–Stokes equations (George 2013). Given this and the prior failed attempts at using Reynolds stress

for predicting hemolysis, we chose not to consider it in the present study.

It is also possible to use an energy dissipation-based effective scalar stress (e.g., see Wu et al. 2019) that incorporates the influence of both the resolved viscous stress and the unresolved stress due to small-scale turbulence. This formulation is advantageous for turbulence-generated hemolysis because, unlike the Reynolds stress, the turbulence dissipation-based stress is a reasonable estimate of the physical stress that RBCs experience at this spatial scale. Using this stress definition, however, only makes a difference in regions of turbulence-generated hemolysis because, as noted by Wu et al. (2019), the energy dissipation-based effective scalar stress *for laminar flow* is equivalent to the resolved viscous stress as we have defined it here in Eq. 3. Given that a large majority of the hemolysis in the FDA nozzle occurs at the sudden contraction of the inlet where the flow is laminar, our use of the latter definition is appropriate. Further, there is the additional complexity that it is not clear what empirical coefficients should be used when  $\sigma$  is defined in terms of a small-scale turbulence-based stress, as nearly all power law coefficients that have been developed to date are for laminar flow. The physical mechanisms through which turbulence causes RBC damage are not well understood, but given the simplistic empirical nature of the hemolysis power law model and the sensitivity of the results to model coefficients, if such a turbulence-based stress formulation is used with the power law model it is likely that the coefficients will need to be calibrated using turbulent flow experimental data in which the influence of small-scale turbulence stresses is isolated. Even so, had we attempted to use such a turbulence dissipation-based stress to predict any turbulence-generated hemolysis in the FDA nozzle, our overall findings would remain the same. Our CFD hemolysis simulations significantly overpredicted the experimental measurements of MIH by roughly three orders of magnitude. Using an energy dissipation-based effective scalar stress (e.g., as in Wu et al. 2019) would yield the same hemolysis predictions due to resolved viscous stress and additional hemolysis generation due to the turbulence contributions, resulting in predictions of even larger values of MIH. For this reason, we chose not to investigate the use of other effective scalar stress formulations that attempt to account for the influence of turbulence.

## Appendix 1: PIV validation and mesh refinement studies

Before comparing LES results with the experiments, we must ensure that the LES time-averaging window is long enough such that the results of interest are statistically converged. Each LES was started by running for  $t = 15$  ms to allow the initial transient from the impulsively started

flow to advect downstream. This time scale was chosen as it represents approximately twice the time required for flow to advect through the nozzle throat. Time-averaging of the LES flow solution commenced at  $t = 15$  ms and continued until  $t = 50$  ms. Temporal convergence of the LES time-averaging was evaluated by comparing the evolution of the normalized axial velocity profiles ( $u_{mean}/U$ , where  $U$  is the mean velocity at the inlet of the nozzle) for  $t = 30, 35, 40, 45$ , and  $50$  ms. This is shown for the fine mesh in Fig. 8 at three axial locations in the nozzle: (a)  $z = -4$  mm (just upstream of the sudden contraction), (b)  $z = 4$  mm (just downstream of the sudden contraction), and (c)  $z = 48$  mm (same cross section in the diffuser where the index of hemolysis is computed). As illustrated, the time-averaged velocity profiles are temporally converged at all locations by a simulation time of  $t = 50$  ms. This, therefore, confirms that averaging for 35 ms is adequate to achieve convergence. All subsequent LES mean flow results are reported using this averaging time window.

The CFD predictions of the flow field from LES and RANS are illustrated in Fig. 9. As expected, both LES and RANS predict that the flow is laminar in the entry region of the nozzle throat, where we anticipate a majority of the hemolysis occurs. This is evident from the instantaneous velocity contours from LES illustrated in Fig. 9(a) and the turbulent viscosity ratio from the RANS simulation in Fig. 9(b), which shows that the  $k-\omega$  SST turbulence model is inactive in this region. Both simulations predict that a small vena contracta forms just downstream of the sharp corner as the flow enters the sudden contraction, followed by the onset of transition to turbulence. Overall, the time-averaged LES velocity field (Fig. 9c) is qualitatively comparable to the RANS solution (Fig. 9d) throughout the nozzle throat. There are differences between LES and RANS, however, in the downstream diverging section of the nozzle, where LES predicts that the jet spreads more quickly than the RANS simulation.

Quantitative comparisons of the mean velocity profiles from CFD and PIV are shown in Fig. 10. At the location of the sudden contraction ( $z = 0$  mm), both LES and RANS predict a blunt, nearly uniform velocity profile as the flow enters the nozzle throat (Fig. 10a). There is little difference between the LES and RANS solutions, consistent with the fact that the flow is laminar here and the turbulence models are largely inactive in this region. There is also no discernible difference between the coarse and fine mesh solutions for both LES and RANS. The CFD solutions compare reasonably well with the PIV measurements, except in the near-wall region where there is large uncertainty in the experimental data that makes a direct comparison difficult. This is likely due in part to the limited PIV measurement resolution, which ranged from 0.11 to 0.176 mm (Hariharan et al. 2011). For comparison, the boundary layer wall-normal spacing

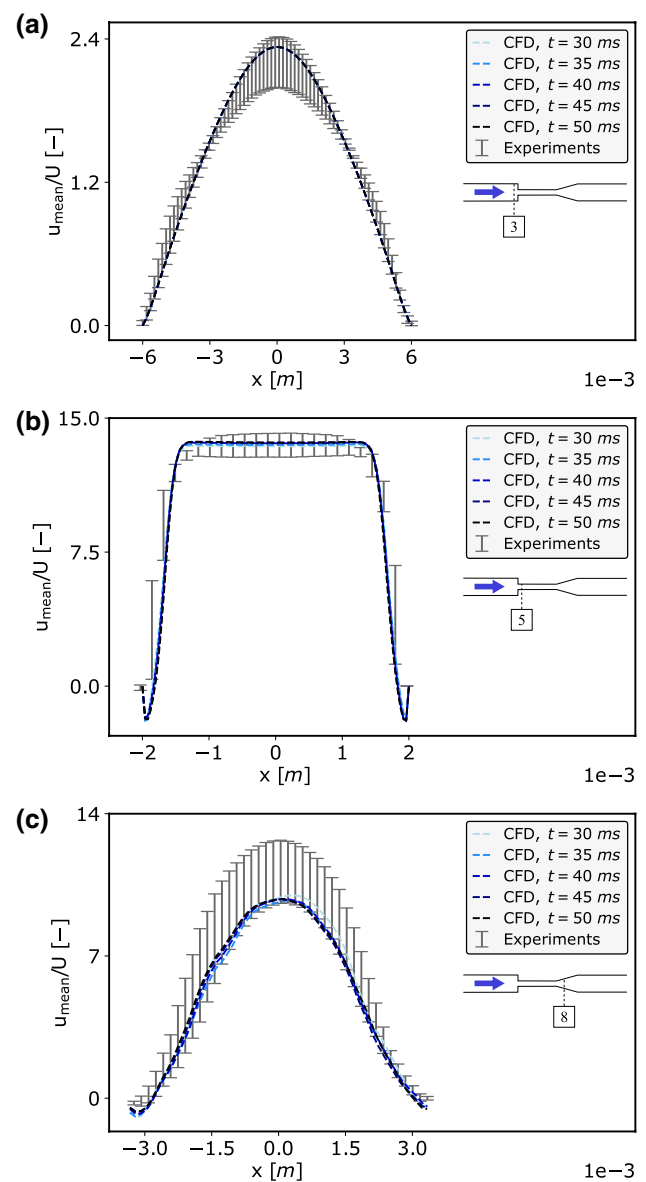


**Fig. 8** Convergence of LES time-averaging using the fine mesh. The evolution of the normalized velocity profile  $u_{mean}/U$  is evaluated at **a**  $z = -4$  mm, **b**  $z = 4$  mm, and **c**  $z = 48$  mm for  $t = 30, 35, 40, 45, 50$  ms. The corresponding PIV velocity profiles from Hariharan et al. (2011) are plotted for reference (shown as mean  $\pm$ SD)

of the coarse and fine CFD meshes is  $1 \mu\text{m}$  and  $0.75 \mu\text{m}$ , respectively. From the CFD simulations, the large near-wall velocity gradient at the sudden contraction occurs over a distance of approximately  $50 \mu\text{m}$ . Thus, the PIV measurements are unable to resolve this steep velocity gradient. Combined with the ambiguity of defining the exact location of the wall in the PIV experiments (Stewart et al. 2013), this explains the large uncertainty in the near-wall PIV data and their limited utility for validating the CFD predictions of near-wall velocity. Even so, the overall comparison is reasonable

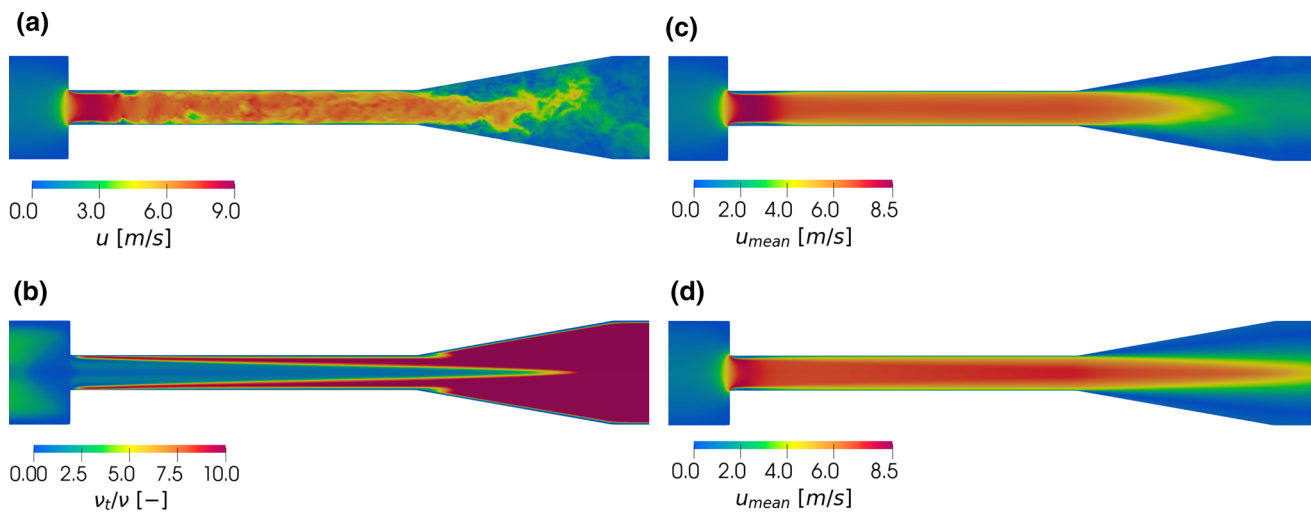


**Fig. 9** CFD predictions of the flow field in the FDA nozzle at  $Re_t = 6500$  from LES and RANS using the fine mesh for each. **a** Instantaneous velocity contours from LES at  $t = 50$  ms. **b** Turbulent

viscosity ratio ( $\nu_t/\nu$ , where  $\nu_t$  is the kinematic turbulent eddy viscosity and  $\nu$  is the kinematic molecular viscosity) from RANS. **c** Time-averaged velocity field from LES. **d** Mean velocity field from RANS

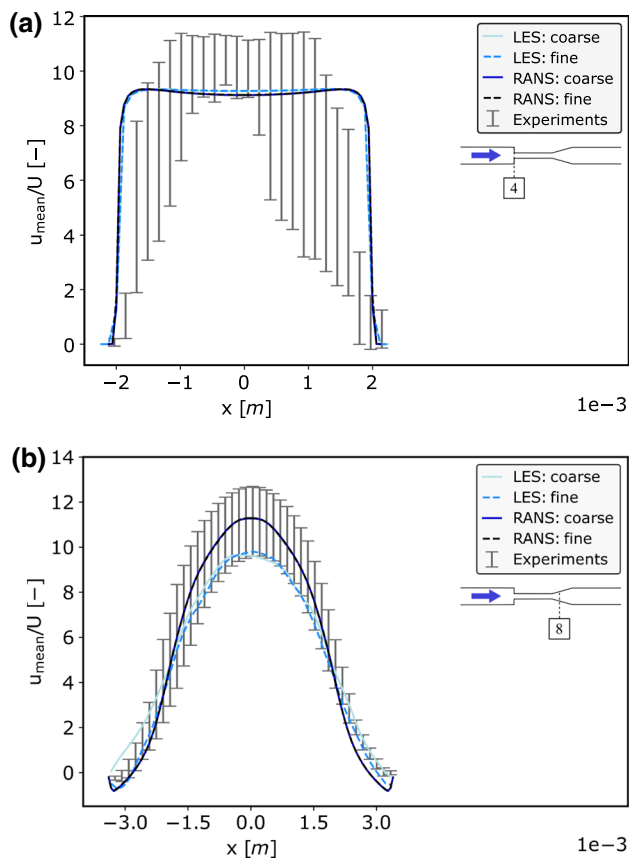


**Fig. 10** Comparison of CFD predictions of the normalized velocity profile  $u_{mean}/U$  in the FDA nozzle at  $Re_t = 6500$  with the PIV measurements of Hariharan et al. (2011) at **a**  $z = 0$  mm and **b**  $z = 48$  mm. The PIV experimental data are shown as mean  $\pm$  SD

and given that the flow is laminar at this location and both LES and RANS predict extremely similar mesh-insensitive solutions here, we believe that this further supports the credibility of the flow simulations in this critical region where a majority of the hemolysis is expected to occur.

We also compare the velocity profiles in the diffuser section at  $z = 48$  mm in Fig. 10(b). As previously mentioned and illustrated in Fig. 9(c,d), LES predicts that the jet in this region spreads more quickly than the RANS simulations, which is observed in the velocity profiles shown in Fig. 10(b). The coarse and fine mesh RANS simulation results are indistinguishable from one another, while there are slight differences between the two LES profiles. Compared with the PIV measurements, both LES and RANS capture the shape of the normalized velocity profile, including the reversed flow near the wall. All CFD profiles are largely within one standard deviation (SD) of the mean PIV measurements, though the RANS profiles are closer to the mean experimental data.

Comparison of the normalized mean velocity along the centerline between CFD and PIV is shown in Fig. 11(a). Here, we see that the centerline velocity increases abruptly in the sudden contraction at  $z = 0$  mm, slightly decreases downstream of the contraction, and then abruptly decreases in the diffuser as the flow decelerates. While both LES and RANS capture the abrupt acceleration at  $z = 0$  mm, LES appears to slightly better predict the peak velocity just downstream of the contraction compared with RANS. In the throat, LES predicts a relatively constant centerline velocity with a magnitude toward the end of the throat that is slightly less than the PIV measurements, while RANS predicts a gradual increase in velocity along the length with a

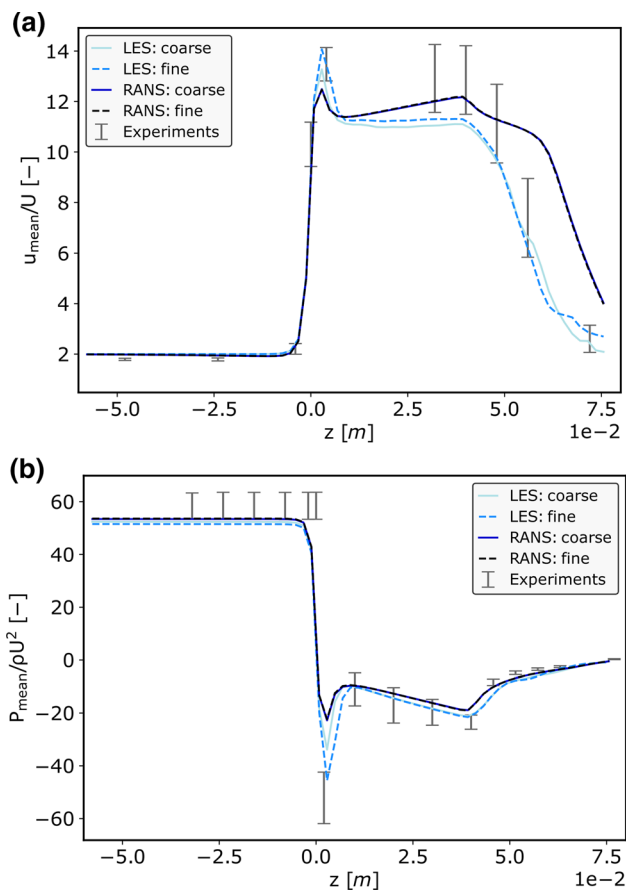


**Fig. 11** Centerline mean velocity and mean wall pressure from CFD compared with experimental measurements in the FDA nozzle at  $Re_t = 6500$ . **a** Normalized mean velocity ( $u_{mean}/U$ ) along the nozzle centerline from LES and RANS compared with PIV measurements (Hariharan et al. 2011). **b** Normalized mean wall pressure ( $P_{mean}/\rho U^2$ ) from LES and RANS compared with experimental pressure measurements (Hariharan et al. 2011). Experimental data are shown as mean  $\pm$  SD

magnitude that better matches the PIV measurements toward the end of the throat. At the beginning of the diffuser section at  $z = 48$  mm, LES and RANS are both within one SD of the mean PIV measurements, though the RANS predictions are closer to the mean experimental data. At farther downstream locations, however, LES is much more accurate in predicting the magnitude of the centerline velocity in the jet compared with RANS, which significantly overpredicts the velocity magnitude.

Comparison of the normalized mean wall pressure between CFD and the experiments is shown in Fig. 11(b). Here, we see that the wall pressure decreases abruptly in the sudden contraction at  $z = 0$  mm, slightly increases downstream of the contraction, gradually decreases along the length of the throat, and then increases in the diffuser. Both LES and RANS wall pressure predictions compare well with the experiments, except just downstream of the

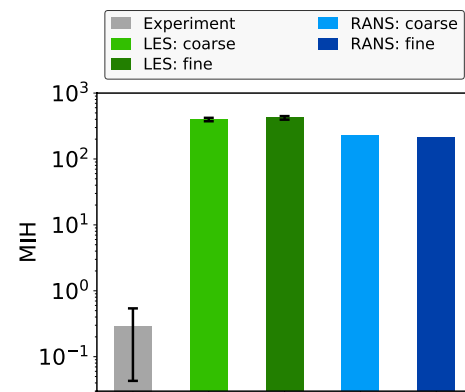


**Fig. 12** CFD mesh refinement study of the modified index of hemolysis (MIH) for the FDA nozzle in the sudden contraction orientation with a blood flow rate of 5 L/min. The CFD simulations use power law model coefficients from Craven et al. (2019). Error bars for LES represent the time-averaged mean  $\pm$  SD. The experimental measurements of Herbertson et al. (2015) are included for comparison (shown as mean  $\pm$  SD)

sudden contraction where LES more accurately predicts the minimum pressure.

Overall, comparing the coarse and fine mesh results, the velocity and wall pressure predictions from the corresponding RANS simulations are indistinguishable from one another. For LES, the fine mesh yields slightly more accurate predictions of velocity and pressure than the coarse mesh. We also performed a mesh refinement study for hemolysis with both RANS and LES using the calibrated power law coefficients. The results are summarized in Fig. 12, where we see that the values of MIH from both RANS and LES are fairly insensitive to the mesh resolution at this level of refinement. Quantitatively, the difference between the coarse and fine mesh hemolysis predictions for both RANS and LES is about 6–7%. As shown in Fig. 12, all of the CFD solutions significantly differ from the experimental measurements of Herbertson et al. (2015).

## Appendix 2: Detailed comparison of FDA nozzle and capillary tube used for calibration

To better understand the reasons for the inaccuracy of the absolute hemolysis CFD predictions, we perform a detailed comparison of several hemolysis-related quantities in the FDA nozzle and the 1-mm diameter capillary tube that was used to calibrate the empirical power law coefficients. Here, we analyze CFD results of the capillary tube from previously reported simulations (Craven et al. 2019) using the same set of power law coefficients used for the FDA nozzle ( $C = 2.875 \times 10^{-10}$ ,  $a = 0.5$ ,  $b = 2.65$ ). We consider the lowest flow rate capillary tube case of Kameneva et al. (2004) because it yields an

average wall shear stress that is approximately the same as that experienced in the FDA nozzle in the sudden contraction orientation at a blood flow rate of 5 L/min. Specifically, Kameleva et al. (2004) quantified their test conditions in terms of the average wall shear stress,  $\bar{\sigma}_{\text{wall}}$ , which was 200 Pa for their lowest flow rate test condition. From our RANS CFD simulation of the FDA nozzle,  $\bar{\sigma}_{\text{wall}}$  in the throat is also approximately 200 Pa.

In comparing the FDA nozzle and the capillary tube, we first examine the velocity magnitude, the effective scalar stress (Eq. 3), and the magnitude of the power law model source term ( $(C\sigma^b)^{1/a}$ ). We also calculate two additional flow-induced stresses that are thought to play an important role in hemolysis. As recently reviewed by Faghiih and Sharp (2019), there is increasing evidence to suggest that the components of the stress tensor beyond simply the scalar magnitude (as expressed in Eq. 3) better correlate with RBC damage. For example, RBCs are thought to be more susceptible to damage caused by extensional (positive normal) stress than shear stress (Faghiih and Sharp 2020). We compare these two stresses in each model by computing the normal and shear stresses experienced by RBCs as they travel through each device. The normal stress ( $\sigma_n$ ) is calculated as

$$\sigma_n = (\boldsymbol{\sigma} \cdot \mathbf{f}) \cdot \mathbf{f} \quad (7)$$

where  $\mathbf{f}$  is the unit vector representing the local flow direction and is defined as  $\mathbf{f} = \mathbf{u}/\|\mathbf{u}\|$ . The local magnitude of the shear stress ( $\sigma_{\text{shear}}$ ) experienced by the RBCs is then calculated as

$$\sigma_{\text{shear}} = [(\boldsymbol{\sigma} \cdot \mathbf{f}) \cdot (\boldsymbol{\sigma} \cdot \mathbf{f}) - \sigma_n^2]^{1/2}. \quad (8)$$

Also, because hemolysis is known to be correlated with the time that RBCs spend at elevated stress levels, we compare the local residence time for the flow through each model by calculating the Eulerian residence time (ERT) (Long et al. 2014; Reza and Arzani 2019). The ERT is computed by solving the following transport equation

$$\frac{\partial \text{ERT}}{\partial t} + (\mathbf{u} \cdot \nabla) \text{ERT} = S_{\text{ERT}}(\mathbf{x}) \quad (9)$$

where

$$S_{\text{ERT}}(\mathbf{x}) = \begin{cases} 1 & \text{if } \mathbf{x} \in \text{region of interest} \\ 0 & \text{otherwise} \end{cases} \quad (10)$$

is the source term defined as the Heaviside function that is unity in the region of interest where the ERT accumulates and zero elsewhere (Long et al. 2014). The boundary conditions include a zero Dirichlet condition at the inlet and a zero-gradient Neumann condition on the walls and the outlet. The ERT region of interest for both the FDA nozzle and the capillary tube begins one diameter upstream of the

inlet of the small diameter section and extends throughout its entire length. Given the computed steady axisymmetric flow solution for each case, the quasi-steady ERT solution was computed in OpenFOAM with the same numerical schemes used for hemolysis (see Sect. 2.6).

We compare the flow-induced hemolysis-related quantities for the FDA nozzle and the capillary tube in Fig. 13. For a flow rate of 5 L/min, the average velocity through the FDA nozzle is 6.6 m/s compared to 3.1 m/s for the capillary tube with a flow rate of 0.148 L/min. Due to the sudden contraction, however, the flow accelerates much more abruptly through the inlet of the FDA nozzle, where a small vena contracta forms at the sharp inlet corner and flow speeds reach approximately 10 m/s (Fig. 13a). This rapid acceleration causes extremely high viscous stresses to develop in a small confined region at the inlet corner (Fig. 13b), with maximum scalar stress ( $\sigma$ ) values of more than  $10^4$  Pa. The scalar viscous stress is, however, much lower elsewhere in the nozzle, with appreciable values being confined to a thin near-wall region where the wall shear stress is 200 Pa. In contrast, the flow accelerates more gradually through the inlet of the capillary tube, resulting in a much lower maximum scalar stress value of approximately 900 Pa. The average wall shear stress in the capillary is also 200 Pa, but appreciable values occur over a much larger relative distance from the wall compared to the nozzle (Fig. 13b).

The differences in the distribution of  $\sigma$  impact the predicted hemolysis generation in each model. The large scalar stress at the inlet corner of the nozzle results in a localized region of extremely high hemolysis generation with a maximum value of approximately  $190 \text{ s}^{-1}$  (Fig. 13c). The generation is, however, much lower elsewhere, most notably in the near-wall region where the highest values are in the range of  $10^{-7} \text{ s}^{-1}$  in an extremely thin region at the wall, with values decreasing quickly just off the wall. In contrast, the highest hemolysis generation in the capillary tube is approximately  $0.0003 \text{ s}^{-1}$  at the inlet lip. Like in the nozzle, the generation is also in the range of  $10^{-7} \text{ s}^{-1}$  along the wall of the capillary, but there is a significant difference in that appreciable generation occurs over a much larger relative distance from the wall compared to the nozzle.

To further elucidate differences in the fluid dynamics that may impact hemolysis, we compare the directional stresses (shear and normal) experienced by RBCs as they travel through the inlet of each device. The distribution of shear stress along the flow direction ( $\sigma_{\text{shear}}$ ) is extremely similar to that shown for the scalar viscous stress,  $\sigma$  (Fig. 13b). There are some notable differences, however, in the distribution of the extensional (positive) normal stress,  $\sigma_n$ . In the FDA nozzle,  $\sigma_n$  is extremely high in a small confined region at the inlet corner (Fig. 13d), where a maximum value of more than  $10^3$  Pa occurs, but decreases quickly with distance away from the corner. As illustrated in Fig. 13(d), the maximum

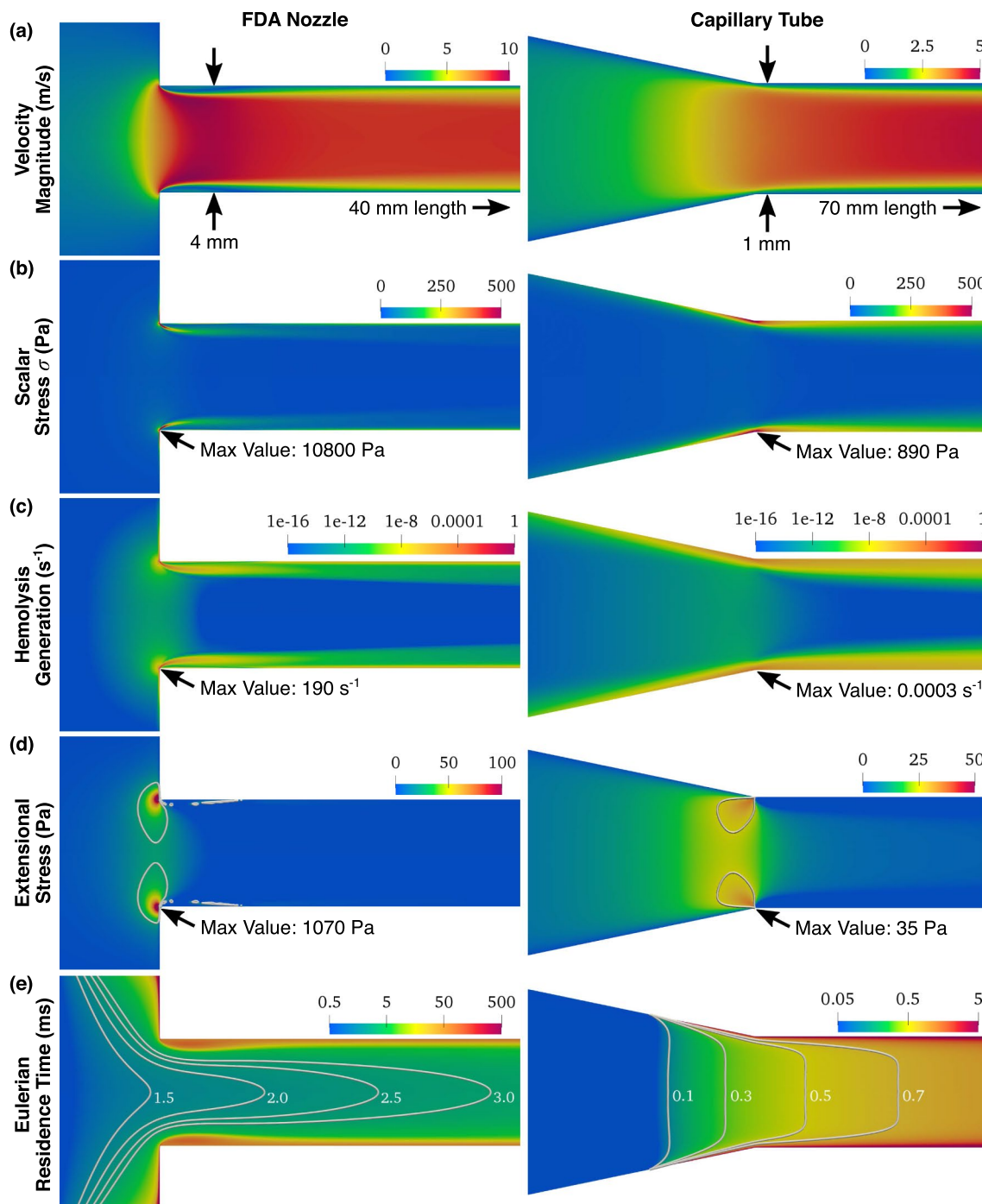


**Fig. 13** Flow-induced hemolysis-related quantities in the inlet of the FDA nozzle (left) and the capillary tube of Kameneva et al. (2004) (right), which was used to calibrate the power law model coefficients used in this study. Comparison of **a** velocity magnitude, **b** effective scalar stress,  $\sigma$ , defined as the magnitude of the viscous stress (Eq. 3), **c** hemolysis generation quantified as the magnitude of the source term in Eq. 2 from simulations using the same set of calibrated coefficients

( $C = 2.875 \times 10^{-10}$ ,  $a = 0.5$ ,  $b = 2.65$ ), **d** extensional stress defined as the positive normal stress (Eq. 7) with contours extracted at 25 Pa, and the **e** Eulerian residence time (Eq. 9) with several contours extracted at the values indicated. In panels **a**, **d**, and **e**, note that the ranges of the contour legends differ for the FDA nozzle and the capillary tube

extensional stress in the capillary tube is only 35 Pa. But, the gradient of  $\sigma_n$  in the vicinity of the inlet lip is much smaller

than in the nozzle such that moderate extensional stresses (e.g., 25–50 Pa) occur over a similar spatial extent and lower

values of  $\sigma_n$  (e.g., 10–25 Pa) occur over an even larger region in the capillary compared to the nozzle.

Comparison of the residence time reveals that RBCs spend slightly more time flowing through the inlet region of the FDA nozzle, but significantly less time flowing along the entire length of the throat section compared to the capillary tube. As shown with the contours of ERT in Fig. 13(e), it takes approximately 0.5 ms to travel one diameter downstream in the center of the nozzle inlet compared to roughly 0.25 ms to travel the same relative distance in the capillary tube inlet. The capillary, however, is much longer than the FDA nozzle. We estimate the characteristic residence time in the small diameter section of each model by calculating  $t \sim L/\bar{U}$ , where  $L$  and  $\bar{U}$  are the length and average velocity, respectively. The characteristic residence time in the 40-mm-long throat section of the FDA nozzle is approximately 6 ms compared to about 22 ms to flow through the 70-mm-long capillary tube.

**Acknowledgments** We thank Luke Herbertson and Kenneth Aycock for reviewing the manuscript and for helpful comments. This work used the Extreme Science and Engineering Discovery Environment (XSEDE), which is supported by National Science Foundation grant number ACI-1548562. The study was funded in part through the NIH NHLBI grant HL146921. NIH did not have any involvement in the study design, in the collection, analysis and interpretation of data; in the writing of the manuscript; and in the decision to submit the manuscript for publication.

## Declarations

**Conflict of interest** The authors declare that they have no conflict of interest.

## References

- Aycock KI, Campbell RL, Lynch FC, Manning KB, Craven BA (2016) The importance of hemorheology and patient anatomy on the hemodynamics in the inferior vena cava. *Ann Biomed Eng* 44(12):3568–3582
- Craven BA, Aycock KI, Manning KB (2018) Steady flow in a patient-averaged inferior vena cava: part ii—computational fluid dynamics verification and validation. *Cardiovasc Eng Technol* 9:654–673
- Craven BA, Aycock KI, Herbertson LH, Malinauskas RA (2019) A CFD-based Kriging surrogate modeling approach for predicting device-specific hemolysis power law coefficients in blood-contacting medical devices. *Biomech Model Mechanobiol* 18(4):1005–1030
- Ding J, Niu S, Chen Z, Zhang T, Griffith BP, Wu ZJ (2015) Shear-induced hemolysis: species differences. *Artif Organs* 39(9):795–802
- Faghih MM, Sharp MK (2019) Modeling and prediction of flow-induced hemolysis: a review. *Biomech Model Mechanobiol* 18:845–881
- Faghih MM, Sharp MK (2020) Deformation of human red blood cells in extensional flow through a hyperbolic contraction. *Biomech Model Mechanobiol* 19:251–261
- Fraser KH, Zhang T, Ertan Taskin M, Griffith BP, Wu ZJ (2012) A quantitative comparison of mechanical blood damage parameters in rotary ventricular assist devices: shear stress, exposure time and hemolysis index. *J Biomech Eng* 134(8):081002
- George WK (2013) Lectures in Turbulence for the 21st Century. Chalmers University of Technology, Available at [www.turbulence-online.com](http://www.turbulence-online.com)
- Giersiepen M, Wurzinger L, Opitz R, Reul H (1990) Estimation of shear stress-related blood damage in heart valve prostheses - in vitro comparison of 25 aortic valves. *Int J Artif Organs* 13(5):300–306
- Goubergrits L, Osman J, Mevert R, Kertzschner U, Pöthkow K, Hege HC (2016) Turbulence in blood damage modeling. *Int J Artif Organs* 39(4):160–165
- Grigioni M, Morbiducci U, D’Avenio G, Benedetto GD, Gaudio CD (2005) A novel formulation for blood trauma prediction by a modified power-law mathematical model. *Biomech Model Mechanobiol* 4(4):249–260
- Hariharan P, Giarra M, Reddy V, Day SW, Manning KB, Deutsch S, Stewart SF, Myers MR, Berman MR, Burgreen GW, Paterson EG, Malinauskas RA (2011) Multilaboratory particle image velocimetry analysis of the FDA benchmark nozzle model to support validation of computational fluid dynamics simulations. *J Biomech Eng* 133(4):1–14
- Heck ML, Yen A, Snyder TA, O’Rear EA, Papavassiliou DV (2017) Flow-field simulations and hemolysis estimates for the Food and Drug Administration critical path initiative centrifugal blood pump. *Artif Organs* 41(10):E129–E140
- Herbertson LH, Salim EO, Daly A, Noatch CP, Smith WA, Kamenewa MV, Malinauskas RA (2015) Multilaboratory study of flow-induced hemolysis using the FDA benchmark nozzle model. *Artif Organs* 39(3):237–248
- Heuser G, Opitz R (1980) A Couette viscometer for short time shearing of blood. *Biorheology* 17(1–2):17–24
- Hund S, Antaki J, Massoudi M (2010) On the representation of turbulent stresses for computing blood damage. *Int J Eng Sci* 48(11):1325–1331
- Kamenewa MV, Burgreen GW, Kono K, Repko B, Antaki JF, Umezu M (2004) Effects of turbulent stresses upon mechanical hemolysis: experimental and computational analysis. *ASAIO J* 50(5):418–423
- Long C, Esmaily-Moghadam M, Marsden A, Bazilevs Y (2014) Computation of residence time in the simulation of pulsatile ventricular assist devices. *Comput Mech* 54(4):911–919
- Malinauskas RA, Hariharan P, Day SW, Herbertson LH, Buesen M, Steinseifer U, Aycock KI, Good BC, Deutsch S, Manning KB, Craven BA (2017) FDA benchmark medical device flow models for CFD validation. *ASAIO J* 63(2):150–160
- Menter F, Kuntz M, Langtry R (2003) Ten years of industrial experience with the SST turbulence model. *Turbul Heat Mass Transf* 4(1):625–632
- Menter FR (1994) Two-equation eddy-viscosity turbulence models for engineering applications. *AIAA J* 32(8):183–200
- Merrill EW, Pelletier GA (1967) Viscosity of human blood: transition from Newtonian to non-Newtonian. *J Appl Physiol* 23(2):178–182
- Nicoud F, Ducros F (1999) Subgrid-scale stress modelling based on the square of the velocity gradient tensor. *Flow Turbul Combust* 62(3):183–200
- Reza MMS, Arzani A (2019) A critical comparison of different residence time measures in aneurysms. *J Biomech* 88:122–129
- Roache PJ (2009) Fundamentals of verification and validation. Hermosa Publishers, Socorro, New Mexico
- Stewart SF, Paterson EG, Burgreen GW, Hariharan P, Giarra M, Reddy V, Day SW, Manning KB, Deutsch S, Berman MR, Myers MR, Malinauskas RA (2012) Assessment of CFD performance in simulations of an idealized medical device: results of FDA’s first

- computational interlaboratory study. *Cardiovasc Eng Technol* 3(2):139–160
- Stewart SF, Hariharan P, Paterson EG, Burgreen GW, Reddy V, Day SW, Giarra M, Manning KB, Deutsch S, Berman MR, Myers MR, Malinauskas RA (2013) Results of FDA's first interlaboratory computational study of a nozzle with a sudden contraction and conical diffuser. *Cardiovasc Eng Technol* 4(4):374–391
- Taskin ME, Fraser KH, Zhang T, Wu C, Griffith BP, Wu ZJ (2012) Evaluation of Eulerian and Lagrangian models for hemolysis estimation. *ASAIO J* 58(4):363–372
- Tobin N, Manning KB (2020) Large-eddy simulations of flow in the FDA benchmark nozzle geometry to predict hemolysis. *Cardiovasc Eng Technol* 11(3):254–267
- Wu P, Gao Q, Hsu PL (2019) On the representation of effective stress for computing hemolysis. *Biomech Model Mechanobiol* 18(3):665–679
- Yu H, Engel S, Janiga G, Thévenin D (2017) A review of hemolysis prediction models for computational fluid dynamics. *Artif Organs* 41(7):603–621
- Zhang T, Taskin ME, Fang HB, Pampori A, Jarvik R, Griffith BP, Wu ZJ (2011) Study of flow-induced hemolysis using novel Couette-type blood-shearing devices. *Artif Organs* 35(12):1180–1186

**Publisher's Note** Springer Nature remains neutral with regard to jurisdictional claims in published maps and institutional affiliations.